

Radial Migration from Metallicity Gradient of Open Clusters and Outliers

HAOPENG ZHANG,^{*} YUQIN CHEN,^{*} AND GANG ZHAO^{*}

ABSTRACT

Radial migration is an important process in the evolution of the Galactic disk. The metallicity gradient of open clusters and its outliers provide an effective way to probe for this process. In this work, we compile metallicity, age, and kinematic parameters for 225 open clusters and carry out a quantitative analysis of radial migration via the calculated migration distances. Based on clusters with age < 0.5 Gyr, we obtain the present-day metallicity gradient of -0.074 ± 0.007 dex/kpc. Along this gradient distributes three sequences, and clusters in the upper, the middle, and the lower groups are found to be old outward-migrators, in-situ clusters, and inward-migrators, respectively. The migration distance increases with age, but its most effective time is probably less than 3 Gyr. The metallicity gradient breaks out at R_g (guiding center radius) ~ 11.5 kpc, which is caused by the lack of young open clusters in the outer disk and the presence of old outward-migrators in the upper sequence. It shows that this boundary is related to the different effects of radial migration between the inner and outer disks. We also found many special open clusters in and near the outer disk of $R > 11$ kpc and a steeper metallicity gradient from the inner disk of $R_g < 7$ kpc, which tells a complicated evolution history of the Galactic disk by different effects of stellar radial migration.

Keywords: Galaxy: abundances – Galaxy: disc – Galaxy: evolution – Galaxy: solar neighbourhood

1. INTRODUCTION

In recent years, with the progress of large-scale surveys in astrometry, e.g. Gaia (Gaia Collaboration 2018), and spectroscopy, e.g. APOGEE (Majewski et al. 2017), GALAH (De Silva et al. 2015), Gaia-ESO (Gilmore et al. 2012), and LAMOST (Deng et al. 2012; Cui et al. 2012), a large number of stars' positions, velocities, ages, and chemical abundances can be obtained, providing the most reliable and detailed observational constraints on the theory of the formation and evolution of the Milky Way. In the Galactic halo, low- α abundance pattern of stellar streams provides evidence on the merging history of the Milky Way with dwarf galaxies in the context of the Λ cold dark matter model (e.g. Nissen & Gustafsson 2018; Helmi et al. 2018). In the Galactic disk, the lack of age metallicity relation indicates an important process of stellar radial migration, which is a recent hot topic in astrophysics (e.g. Bergemann et al. 2014; Minchev et al. 2018).

According to Sellwood & Binney (2002), the interaction between the star and the transient spiral arm will cause the angular momentum to change, and the star's guiding center will also change

^{*} CAS Key Laboratory of Optical Astronomy, National Astronomical Observatories, Beijing 100101, China
School of Astronomy and Space Science, University of Chinese Academy of Sciences, Beijing 100049, China

accordingly. [Minchev & Famaey \(2010\)](#) and [Minchev et al. \(2011\)](#) proposed a new mechanism for radial migration, which is caused by the nonlinear resonance overlap between the central bar and spiral arms of the galaxy. In addition, the disturbance caused by minor mergers can also give rise to radial migration (e.g. [Quillen et al. 2009](#); [Bird et al. 2012](#)). Minor mergers usually play a role in the outer disk, but they strengthen the structure of the spiral arms and bars, thereby indirectly affecting the entire disk (e.g. [Gómez et al. 2012](#); [Minchev et al. 2013](#)).

For a long time, open clusters are widely used to trace the evolution of the Galactic disk. Since the ages and chemical composition of open clusters can be determined with higher accuracy than field stars, they are better tracers of the variation with time of the Galactic properties, and they can be useful to study the effect of radial migration with time. However, we should recall that open clusters are more massive than single stars, and thus the effect of the interactions with spiral arms, bars, etc. might be different and less pronounced. In this respect, [Anders et al. \(2017\)](#) first suggested that open clusters experience significant radial migration. [Minchev et al. \(2018\)](#) and [Quillen et al. \(2018\)](#) proposed that radial migration is expected to flatten the radial metallicity gradient on a long enough time scale. Using the catalog of [Netopil et al. \(2016\)](#), [Chen & Zhao \(2020\)](#) calculated the migration distances for 146 open clusters and found that 56% of the open clusters had migrated. They measured the migration rate 1.5 ± 0.5 kpc/Gyr from intermediate-age open clusters in the outer disk, and found a fraction of clusters tend to migrate inward.

In this work, we aim to increase the number of open clusters by combining multiple spectroscopic survey data into the catalog of [Netopil et al. \(2016\)](#), and investigate how radial migration introduces scatter in the metallicity gradient and what outlier clusters in the metallicity gradient tell us different mechanisms of radial migration. Moreover, since [Netopil et al. \(2016\)](#) included mainly nearby clusters, the inclusion of more spectroscopic data in this work will enlarge the sky coverage, and thus provides sufficient data for studying the radial migration of the galactic disk, especially the outer disk.

2. DATA AND METHODS

Metallicity and age are two important parameters for estimating the birth sites of stars, which are required in studying the radial migration of the Galactic disk. Based on color-magnitude diagrams from high precision photometries, the ages of most open clusters are available in the literature. However, only a small percentage of open clusters have reliable metallicities in the literature due to the lack of spectroscopic data for many clusters. [Netopil et al. \(2016\)](#) provided a homogeneous sample of nearby open clusters with compiled metallicities from previous works. They used high-resolution spectroscopic, low-resolution spectroscopic, and photometric data to derive the metallicity of 172 open clusters. We integrate this sample and only use high-resolution spectroscopic data to ensure the reliability of metallicities. For these clusters, [Soubiran et al. \(2018\)](#) based on Gaia DR2 provided radial velocities. This sample is the same as that of [Chen & Zhao \(2020\)](#), but we perform a more strict check on metallicity by comparing their values to other works.

With the recent release of high-resolution spectroscopic surveys, including APOGEE, GALAH, Gaia-ESO, more open clusters have reliable metallicities and can be included in the study of radial migration of the disk. [Casali et al. \(2019\)](#) determined the metallicity and radial velocity of 17 open clusters from Gaia-ESO data. [Donor et al. \(2020\)](#) released the metallicity and radial velocity of 128 open clusters in Open Cluster Chemical Abundances and Mapping (OCCAM) survey IV, which are based on APOGEE DR16. [Spina et al. \(2021\)](#) obtained chemical abundances of 134 open clusters

and kinematic properties of 226 open clusters from GALAH+ and APOGEE DR16 data. In addition, the Stellar Population Astrophysics (SPA) survey can also provide chemical and kinematic information from high-resolution spectra of 6 open clusters (see [Frasca et al. 2019](#); [D’Orazi et al. 2020](#); [Casali et al. 2020](#)). For clusters in common in different samples, we prefer to use the value that using more member stars to determine the metallicity to enhance the reliability of the data. We cross-match these samples with the cluster catalog of [Cantat-Gaudin et al. \(2020\)](#) based on Gaia DR2, which can provide the distance, proper motion, and age of these clusters.

Finally, the LAMOST DR7 data can provide a large number of member stars’ spectroscopic data, including metallicity and radial velocity. We cross-match the LAMOST DR7 data with the list of member stars of open clusters from [Cantat-Gaudin et al. \(2020\)](#), and all stars with a membership probability not less than 0.7. The method is the same as in [Zhong et al. \(2020\)](#), who obtained a catalog of 295 open clusters based on the LAMOST DR5, but we have stricter selections by limit each star with the uncertainty of $[\text{Fe}/\text{H}] < 0.15$ dex and the uncertainty of radial velocity < 10 km/s. If the number of cluster members is greater than three, we calculate the average values (and standard deviations) of the metallicity and radial velocity. Then we cross-match this sample with the cluster catalog of [Cantat-Gaudin et al. \(2020\)](#) to obtain distance, proper motion, and age information. We use this sample as a supplement when open clusters were not included in high-resolution spectroscopic data.

In order to ensure the accuracy of the following calculation, we require the uncertainty of the clusters’ metallicities and radial velocities to be less than 0.15 dex and 10 km/s. As we are interested primarily in the thin disk, we only use the sample with $|Z| < 0.5$ kpc (Z is the coordinate in a Galactocentric cylindrical coordinate system) in the following analysis to ensure that the metallicity gradient can be used to estimate their birth sites. Because most of the metallicities of clusters come from [Spina et al. \(2021\)](#), we compare the metallicities from [Donor et al. \(2020\)](#), [Netopil et al. \(2016\)](#), [Casali et al. \(2019\)](#), and LAMOST DR7 with those from [Spina et al. \(2021\)](#), and derive the metallicity calibrations based on clusters in common by linear fits to the data, as shown in red solid lines of Fig. 1. We do not calibrate the metallicities from the SPA survey because this sample is too small. With these calibrations, we obtain a total sample of 231 open clusters with metallicities on the same scale.

3. ANALYSIS

3.1. *Three sequences in the radial metallicity gradient*

Quantitative analysis on the effect of radial migration requires kinematical and orbital parameters to calculate birth sites and migration distances. We thus use galpy ([Bovy 2015](#)) to calculate the orbital parameters of the clusters. The gravitational potential in galpy used in our work is MWPotential2014, rescaled such that $R_{\odot} = 8.178$ kpc ([Abuter et al. 2018](#)), $Z_{\odot} = 25$ pc ([Bennett & Bovy 2019](#)), and the circular velocity is 229 km/s ([Eilers et al. 2019](#)). We adopt the solar motion relative to the local standard of rest of (11.1, 12.24, 7.25) km/s ($U_{\odot}, V_{\odot}, W_{\odot}$, [Schönrich et al. 2010](#)). We calculate several orbital parameters of the clusters, such as R_g (guiding center radius) and peri-/apo-center distances. We use the observational uncertainties of each cluster to calculate the errors of R_g through 1000 MC runs, and the median is 0.04 kpc.

Since the star’s guiding center is a good proxy for the current orbital distance ([Chen & Zhao 2020](#)), which is not altered by blurring, and churning leads to a change in the star’s guiding center

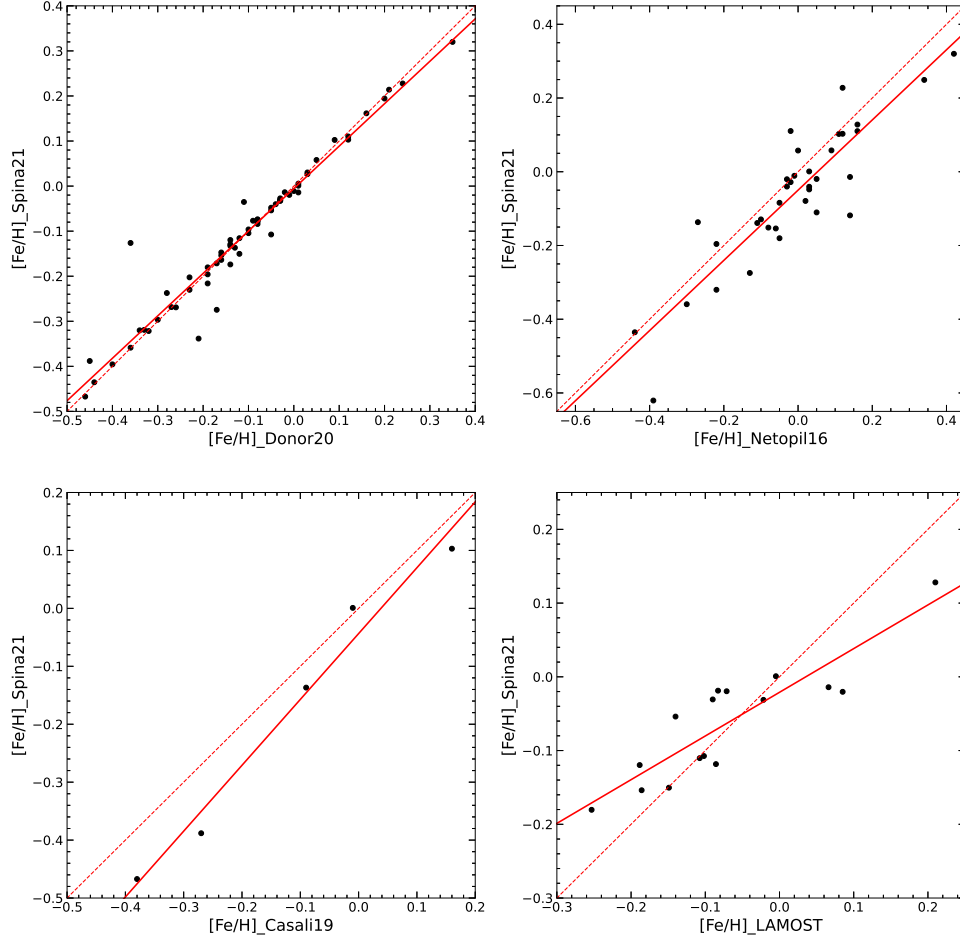


Figure 1. The metallicity calibrations between Spina et al. (2021) and Donor et al. (2020), Netopil et al. (2016), Casali et al. (2019), and LAMOST DR7 based on common clusters. Red solid lines are linear fits to the data and red dash lines show the one-to-one relations.

(Sellwood & Binney 2002), so we will use R_g rather than R to analyze the radial metallicity profile of open clusters. Fig. 2 shows the radial metallicity gradient for the whole sample with an X-axis of R_g . There are six clusters that deviate far from the general trend, and they are marked by their names in the three dashed boxes. Among these clusters, King 12, NGC 6383, NGC 2311, and Berkeley 18 have only one member star in Donor et al. (2020) and Spina et al. (2021), so the value could be uncertain. Note that the metallicity of Kopensov 63 is -0.58 dex in Spina et al. (2021) based on only one member star, while Zhong et al. (2020) gave $[Fe/H] = -0.08$ dex (determined by three members). If we adopt the latter, it does not deviate from the general trend anymore. The metallicity of Berkeley 32 is reliable based on 11 member stars in Netopil et al. (2016) and is close to the value of -0.29 dex by Dias et al. (2002). Thus, Berkeley 32 is a special cluster and will be discussed in Sect. 4.

Excluding these clusters in the three dashed boxes, we obtain a total sample of 225 open clusters, and we perform a running average metallicity for the remaining clusters, using a similar approach as [Genovali et al. \(2014\)](#) and [Netopil et al. \(2016\)](#), by grouping the sample into a constant number of 15 clusters or a maximum distance range of 1.5 kpc, whichever criterion is met first. The result of the running average is shown by red solid curves in Fig. 2. The clusters in the dashed boxes deviate from the running average by at least 3σ , which also confirms their specialty. For comparison, we perform a linear fit to the clusters with $R_g < 10$ kpc, and get a gradient of -0.071 dex/kpc. In general, the two sets of data are consistent until $R_g = 11.5$ kpc, beyond which the radial metallicity gradient begins to flatten out, and there is a significant discrepancy at $R_g \sim 13$ kpc. The reason for this discrepancy is a hot topic for decades, but still an unsolved question today. We also find that the radial metallicity gradient is steeper at $R_g < 7$ kpc, which will be discussed in Sect. 3.4. Usually, the linear fitting gradient is significantly affected by clusters on both sides in different samples, and thus the running average may represent a more reasonable relation between $[\text{Fe}/\text{H}]$ and R_g .

In this work, we avoid to investigate how the metallicity gradient flattens out in the outer disk, since we have only six open clusters at $R_g > 13$ kpc, and they have a wide metallicity range of $[\text{Fe}/\text{H}]$ from -0.35 to -0.1 dex. Instead, we would like to analyze the metallicity scatter at a given R_g in more detail. Generally, the scatter in metallicity is quite similar for all R_g , in the order of 0.08 dex but with a wide range of 0.4 dex, which is larger than the uncertainty in metallicity of 0.05 dex in high-resolution spectroscopic samples (the main part of our data). It is suggested that radial migration has significant contributions to the scatter in the $[\text{Fe}/\text{H}]$ versus R_g diagram. According to [Donor et al. \(2020\)](#), the metallicity at a given Galactocentric distance fits well with the model prediction of [Chiappini \(2008\)](#) (without taking into account radial migration) for young clusters (age < 0.8 Gyr), but it deviates significantly from this model prediction for older clusters. This deviation becomes more significant for the oldest clusters (age > 2.0 Gyr) and is thought to be the evidence for radial migration.

Interestingly, we notice that open clusters below the dashed line seem to form a (lower) sequence parallel to the red dash line, as shown by the green dash line, which indicates that clusters with lower metallicity at the same R_g also have the same gradient as the total sample. Accordingly, we suggest that open clusters above the red dash line may represent another (upper) sequence, as shown by another green dash line. Note that the upper sequence is also found to be a separated one consisting of old clusters with age > 2 Gyr in [Donor et al. \(2020, Fig. 13\)](#) based on high-quality data of 71 open clusters. But they do not have clusters in the lower sequence. We check our data in the lower sequence, and they have consistent metallicities in the literature. Moreover, they do not show more considerable uncertainties in metallicity than the upper sequence. Thus, we suggest that the lower sequence may be real, rather than a false feature from unreliable data. In the MCM chemo-dynamical simulation ([Minchev et al. 2013, 2014](#)), data below the theoretical prediction of [Chiappini \(2008\)](#) exist (as well as data above) as a result of radial migration, which supports the reality of the lower sequence in our work.

3.2. *The age distributions of the three sequences.*

The age metallicity relation for the total sample is shown in Fig. 3. The $[\text{Fe}/\text{H}]$ range of clusters is -0.4 to 0.3 dex, the R_g range of 6 – 15 kpc, and the range of age is 0 to 8 Gyr. As expected, there is no age metallicity relation as already shown by many previous works (e.g. [Carraro & Chiosi 1994](#); [Friel et al. 2010](#); [Yong et al. 2012](#)). In particular, for the youngest clusters of age < 0.5 Gyr, there is

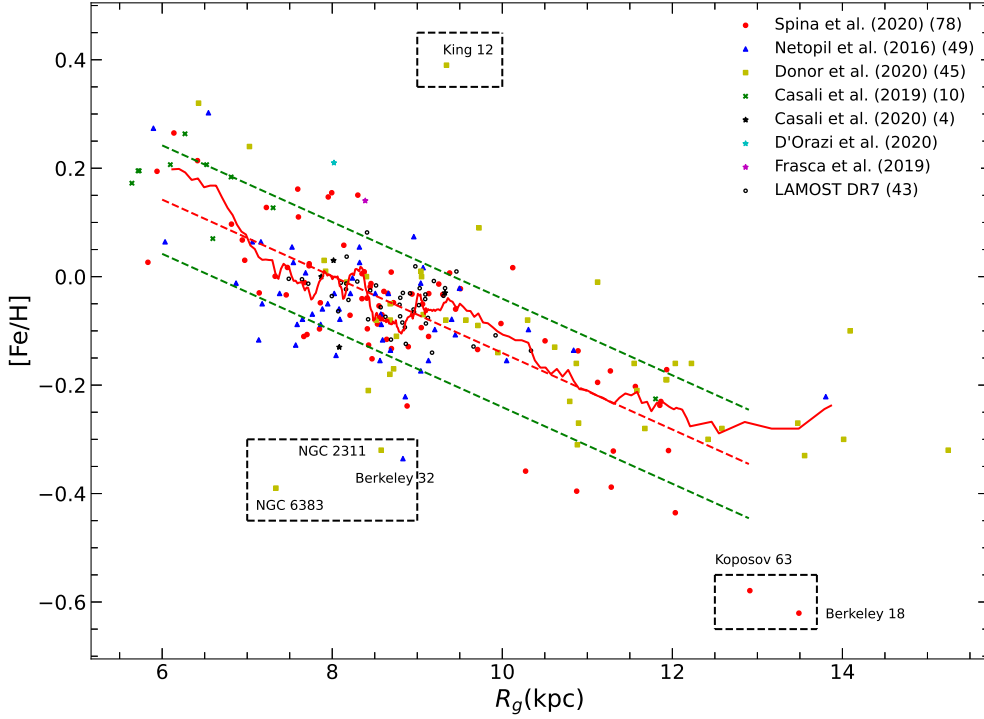


Figure 2. The radial gradient of metallicity for open clusters, different symbols indicate different sources of metallicities. The clusters within the dashed box deviate from the radial gradient and are eliminated in the following work. The red solid line is the running average curve with the samples outside the dashed boxes, and the red dashed line is the linear fit to the $R_g < 10$ kpc samples, as discussed in the text. The green dashed line is obtained by shifting the red dashed line up and down by 0.1 dex.

a $[\text{Fe}/\text{H}]$ range from -0.3 to 0.3 dex, almost as large as the whole sample. This is also the case for clusters with age ~ 4 Gyr. In different R bins ($R \leq 9$, $9 < R \leq 12$, $R > 12$ kpc), there is also no obvious age metallicity relation, only the mean metallicity decreases from the inner to the outer disk (see Fig. 3, below). The age metallicity relation of open clusters with age < 4 Gyr is similar to that of the theoretical models. For example, in the input chemical model of Minchev et al. (2013), the difference of $[\text{Fe}/\text{H}]$ between the present epoch and 4 Gyr ago is 0.17 dex in the solar neighborhood, which is smaller than the scatter. However, for several clusters with age > 5 Gyr, their metallicities are significantly higher than the theoretical values, which suggests that they may be related to radial migration.

Since radial migration requires time to take effect, young clusters are preferred for establishing the radial metallicity gradient. In view of this, we select the clusters with age < 0.5 Gyr and try to estimate the present-day metallicity gradient based on only high-resolution spectroscopic data to ensure the reliability of metallicities, and we require at least three member stars for each cluster. A linear fit to the data gives -0.074 ± 0.007 dex/kpc, which is consistent with that of Donor et al. (2020) (-0.068 dex/kpc for $R_{gc} < 13.9$ kpc, R_{gc} is the Galactocentric distance). The linear fit depends significantly on the points on both sides. Meanwhile, even for clusters with age < 0.5 Gyr,

several open clusters belonging to the upper and lower sequences persist, which indicates that radial migration has a very short timescale. Therefore, it is not wise to limit the cluster's age to get a reliable present-day metallicity gradient. Instead, we attempt to include more clusters that do not suffer from significant radial migration in their lives. This is actually the advantage of using the running average method, which avoids the dependence of few points on both sides and reflects the mean metallicity of local-born clusters (assuming that the majority of clusters were born in local). Note that our derived value of -0.074 dex/kpc is close to the linear fit of -0.071 dex/kpc in Fig. 2, and both are consistent with the running average in the range of $R_g = 7 - 11.5$ kpc.

With the help of the derived present-day metallicity gradient, we select a middle sequence by a shift of 0.05 dex (corresponding to the error in metallicity) upward and downward, and then the upper and lower clusters are the remaining clusters in the upper and lower sequences as shown in Fig. 5. The upper sequence is consistent with Donor et al. (2020), who suggests that the high metallicity results from their origins of inner Galaxy and then migrated radially outwards to present locations. On the contrary, the lower sequence indicates that they are inward-migrated clusters from the outer disk, which will be confirmed in terms of migration distance later. The cumulative curves for the three sequences in Fig. 5 indicate that the upper sequence is obviously older than the middle sequence. As in the middle sequence, more than half of the clusters in the lower sequence are younger than 0.5 Gyr. The difference is that there are also many clusters older than 2 Gyr in the lower sequence. Different age effects between the outward and inward clusters may indicate different timescales or different mechanisms of radial migration.

Fig. 6 shows the distributions of clusters in the three sequences in the Galactic plane. It shows that the upper sequence has the largest distribution range and can be distributed outside the Outer Arm. The middle sequence corresponds to the in-situ clusters clump at the solar location near the Local Arm ($X = 8.2$ kpc, $Y = 0$ kpc), and there is no cluster near the Outer Arm. The distribution of the lower sequence is similar to that of the middle sequence. Again, these distributions indicate that the effect of radial migration is related with age. The upper sequence includes more old clusters and thus can have a large migrated coverage of radial Galactic radius.

3.3. Migration distance as a function of age

We use ISM metallicity variation with time at the solar radius and the ISM metallicity gradient variation with time from Minchev et al. (2018) to calculate the birth radius (R_b) of clusters. Minchev et al. (2018) adopts a semi-empirical and largely model-independent method, which is based on the assumption of ISM metallicity distribution in the disk and AMBRE:HARPS and HARPS-GTO high-quality datasets to deduce the evolution of ISM metallicity gradient with time. This is a good alternative approach in the absence of ISM related data, because the method of Minchev et al. (2018) is also based on observation data. It should be noted that an important assumption of Minchev et al. (2018) is that the ISM is well mixed at a given radius. The result of Nieva & Przybilla (2012) using early B-type stars are consistent with this assumption. Using the HII regions data of 88 galaxies, Zinchenko et al. (2016) proposed that there is no significant global azimuthal asymmetry of $[O/H]$ for their sample, usually lower than 0.05 dex, although some other works analyzing in the Milky Way (Balsler et al. 2015) or individual external galaxies (Sánchez et al. 2015) indicate otherwise. Sánchez et al. (2015) used NGC 6754 to conclude that the variation of oxygen abundance with azimuth is more obvious in the external Galactic regions, and the maximum scatter range of $[O/H]$ at a given radius is about 0.2 dex. Considering that this effect is symmetric around the mean, and

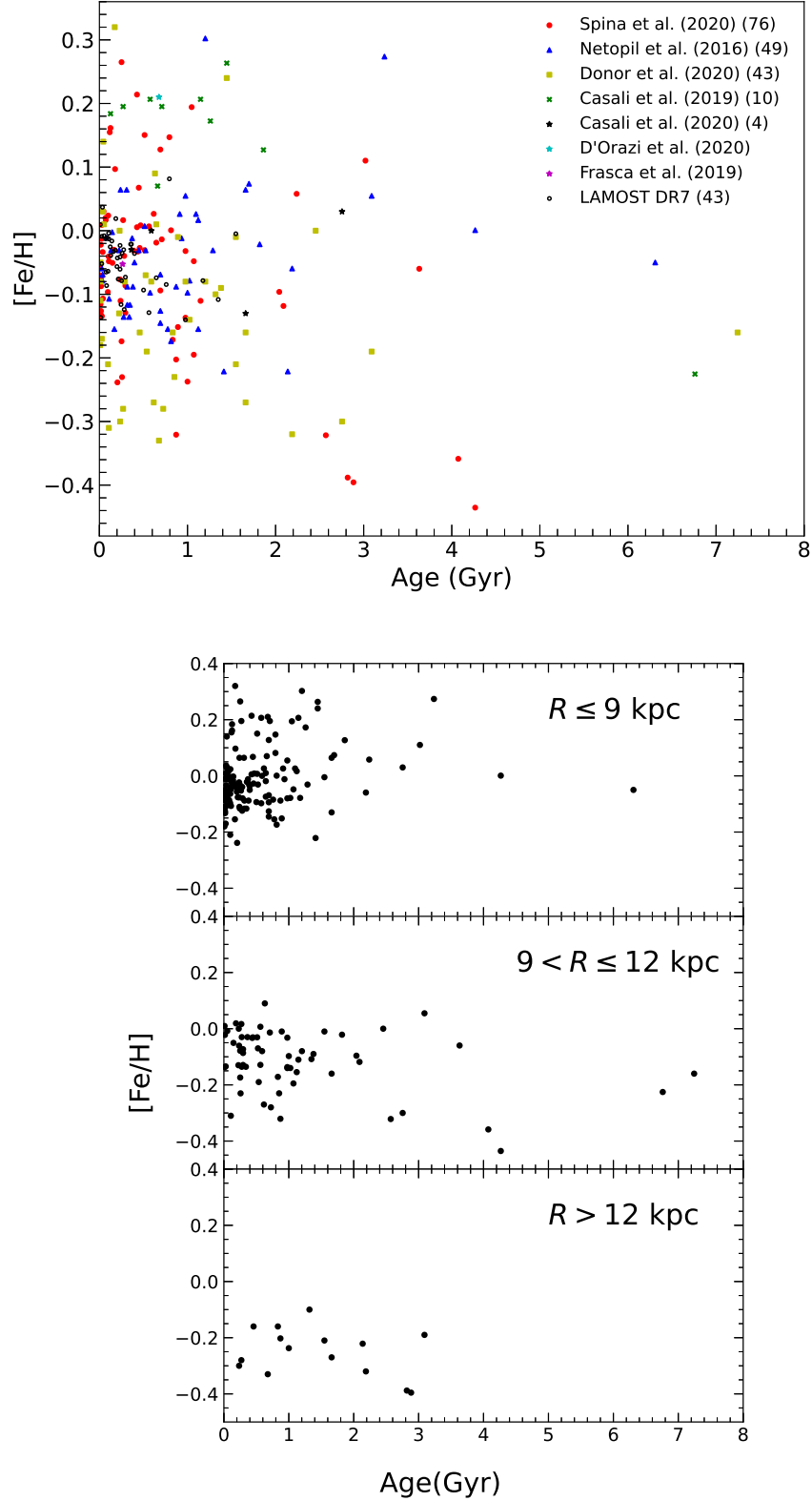


Figure 3. The age-metallicity relation for open clusters, the symbols are the same as in Fig. 2. The clusters within the dashed boxes in Fig. 2 have been eliminated. Age-metallicity relations for different R bins ($R \leq 9$, $9 < R \leq 12$, $R > 12$ kpc) are shown in the lower panel.

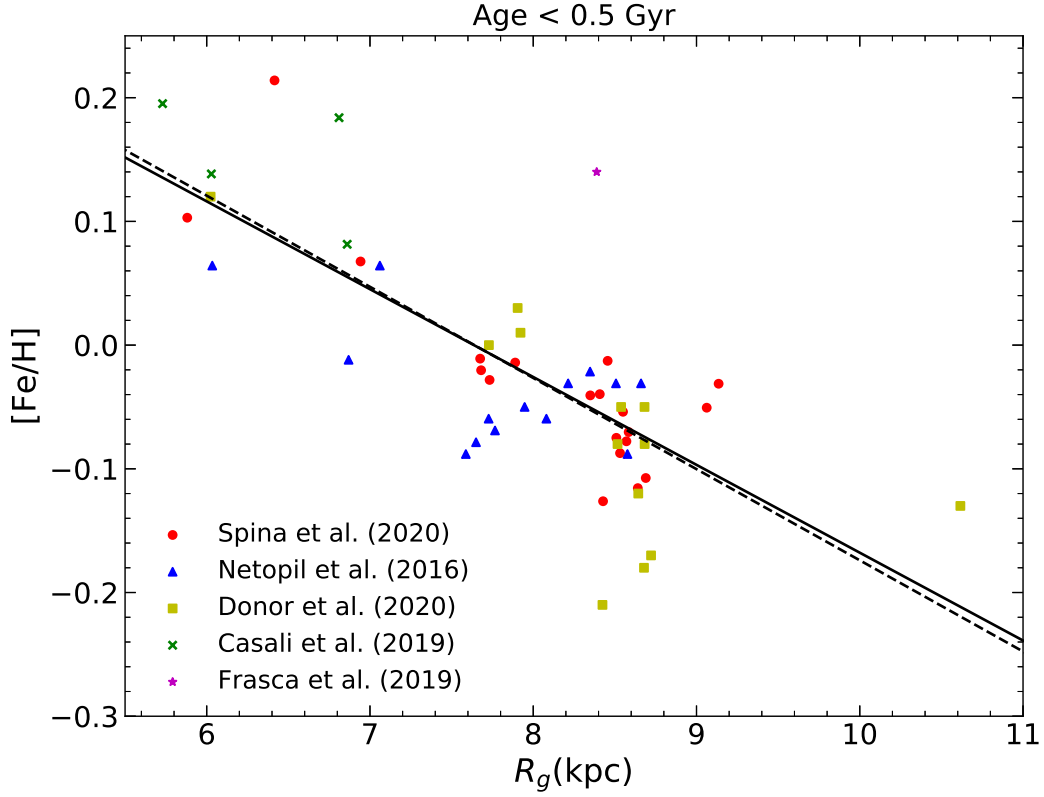


Figure 4. Metallicity as a function of R_g for young clusters (age < 0.5 Gyr) obtained by high-resolution spectroscopic data, different symbols indicate different sources of metallicities. The black dashed line is the linear fit to the data. The black solid line represents the current interstellar medium (ISM) radial metallicity distribution given by [Minchev et al. \(2018\)](#), which has been rescaled downward by 0.14 dex.

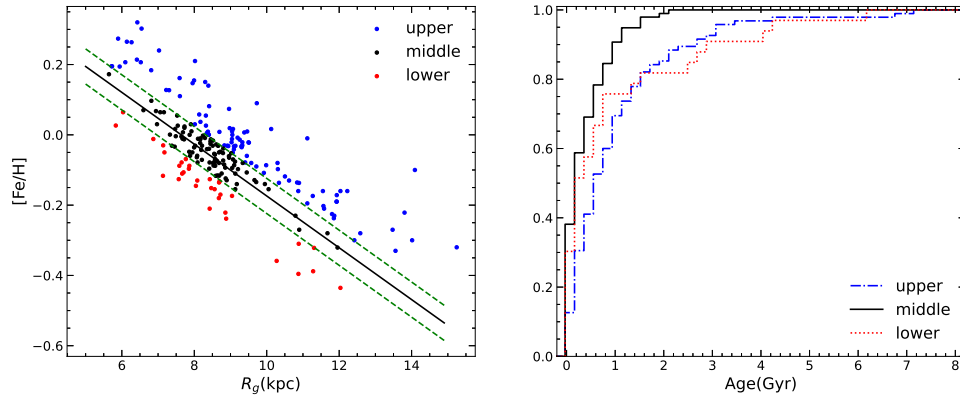


Figure 5. The separation of the lower (red) and upper (blue) sequences by selecting the middle sequence (black) along the present-day metallicity gradient with a shift of 0.05 dex in metallicity. The cumulative curves are shown in the right panel.

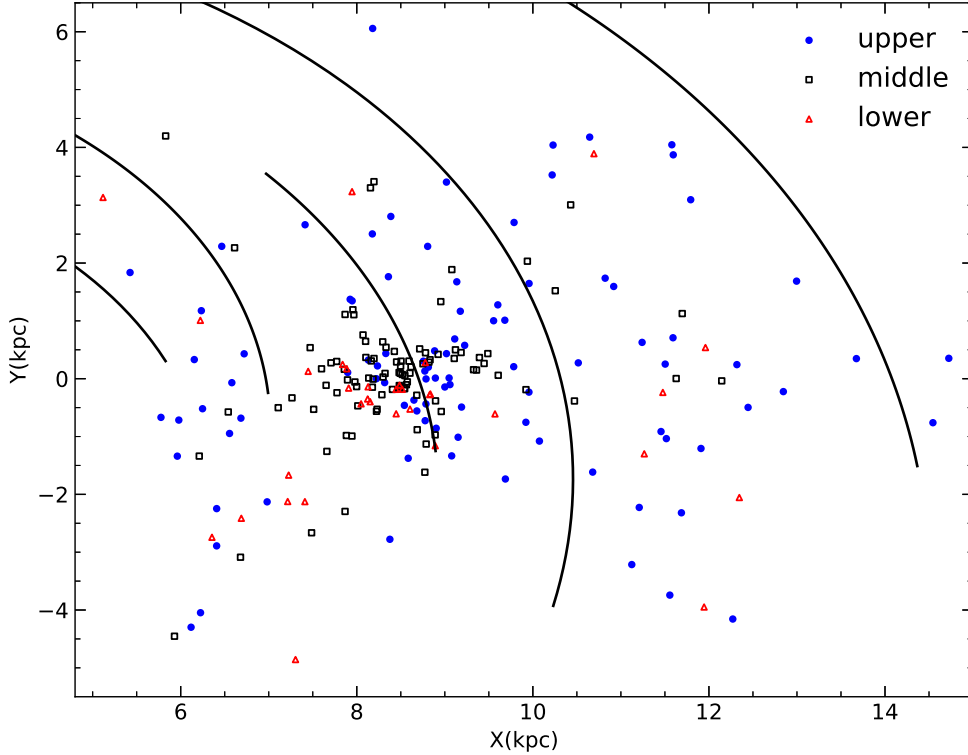


Figure 6. Galactic location of the upper, middle, lower sequences projected to the Galactic plane. The Galactic center is located at $(X/Y) = (0/0)$ kpc and the Sun at $(X/Y) = (8.2/0)$ kpc. The black solid lines indicate the spiral arm model given by Reid et al. (2014, Table 2). The spiral arms from the inner to the outer area are Scutum, Sagittarius, Local, Perseus, and Outer.

most of the open clusters in our sample are in the solar neighborhood rather than in the external regions of the Milky Way, we think the assumption of Minchev et al. (2018) is reasonable. However, this profile obtained by Minchev et al. (2018) using field stars may be systematically different from the samples of the open clusters. As shown in Fig. 4, for the youngest open clusters with ages of $0 - 0.5$ Gyr, according to linear fit, the $[\text{Fe}/\text{H}]$ of the open clusters at solar radius is -0.04 dex, while it is 0.1 dex in Fig. 5 of Minchev et al. (2018). We thus shift the ISM metallicity at the solar radius downward by 0.14 dex in subsequent analysis. This will cause a shift of birth site toward the inner Galaxy for the upper sequence, and a smaller number of clusters in the lower sequence suffer from inward radial migration. The median error of R_b is about 0.5 kpc based on 1000 MC runs, using the age and metallicity uncertainties for each cluster.

In this work, the deviation of R_g from the birth site of R_b is defined to be the migration distance (MD) due to churning, and the deviation of present location R from R_g is due to blurring. Fig. 7 shows the migration distance MD and $R - R_g$ as a function of age. It is obvious that churning is more significant than blurring: about half of the clusters have $|R_g - R_b| > 1$ kpc, but only 14 clusters lie above $|R - R_g| = 1$ kpc. Blurring has an evenly distribution around the median $R - R_g$ of 0.06 kpc, almost close to zero. However, there is an increasing average of $|R - R_g|$ with age. For clusters with

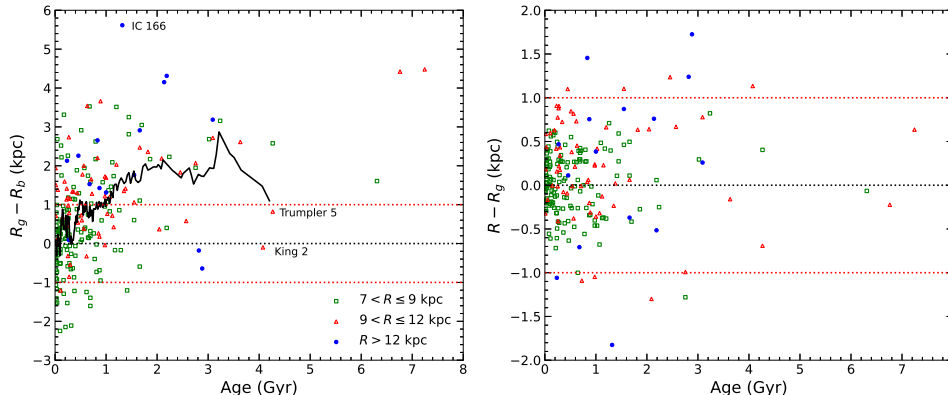


Figure 7. The migration distance $R_g - R_b$ (left) and $R - R_g$ (right) versus age for different Galactic radii R bins. The black solid line in the left panel is the running average curve with all clusters.

$t \leq 0.5$, $0.5 < t \leq 1.0$, $1.0 < t \leq 2.5$, $t > 2.5$ Gyr, the mean $|R - R_g|$ are 0.30, 0.38, 0.49, 0.71 kpc, respectively. This means that blurring does not cause significant displacement in the radial distance, but it does become more effective for old clusters.

In this work, we define $|MD| > 1$ kpc as a migrator, and $|MD| \leq 1$ kpc as an in-situ cluster, based on the median error in MD of 0.5 kpc and above 90% clusters having errors less than 1 kpc. With this definition, 46% of the open clusters are migrators, and 33% of the youngest clusters with age ≤ 0.5 Gyr have migrated, either inward or outward. In order to further analyze the change of the migration distance with age, we performed a running average using the same method as in Sect. 3.1. We adopt a maximum age range of 1 Gyr in the second criterion. The running average curve is shown as black solid curves in the left panel of Fig. 7. The average migration distance increases with age at age < 3.2 Gyr from 0 kpc to 2.9 kpc, leading to the migration rate of approximately 1 kpc/Gyr, which is similar to that estimated by Quillen et al. (2018) (1 kpc/Gyr) based on the Gaussian bar model in Comparetta & Quillen (2012), and this result is slightly smaller than that of Chen & Zhao (2020) (1.5 kpc/Gyr). The migration rate decreases at age > 3.2 Gyr. We do not have enough old clusters in this analysis, and thus, this black line stops at 4 Gyr. It seems that the most effective time of radial migration occurs at around the initial 3 Gyr, with the migration rate of 1 kpc/Gyr. If the results of our analysis are confirmed, this period may be related to the time scale of radial migration caused by the interaction between the bar and spiral arms in Minchev et al. (2013). Further work is desiring to confirm this suggestion. In the left panel of Fig. 7, there are three clusters that deviate from other clusters. We have marked their names in the figure and will discuss them in Sect. 4 as special clusters.

We also show the MD distributions for different age bins in Fig. 8. For clusters with $t \leq 0.5$, $0.5 < t \leq 1.0$, $1.0 < t \leq 2.5$, $t > 2.5$ Gyr, the mean MD are 0.28, 0.88, 1.66, 2.00 kpc, respectively. Again, we see the increase of the migration distance with age. Although quite a large fraction of young clusters migrate inwards, which reduces the mean value of MD in the first two age bins, the general trend of increasing MD with age is valid and this is expected for radial migration, which requires time to move from one place to another.

3.4. Migration Distance as a function of R_g

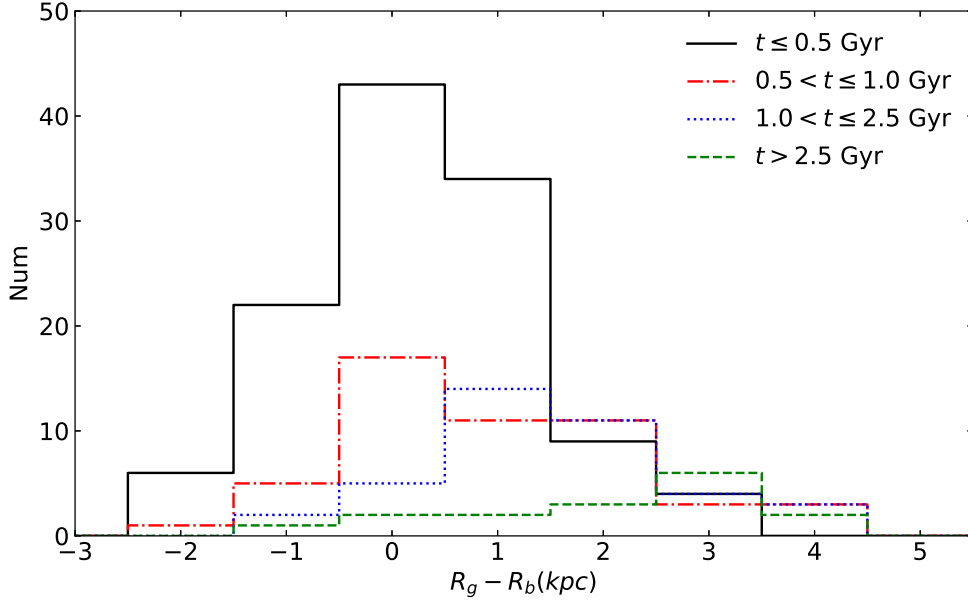


Figure 8. The distributions of migration distance for different age bins: $t \leq 0.5$ Gyr (black solid line), $0.5 < t \leq 1.0$ Gyr (red chain line), $1.0 < t \leq 2.5$ Gyr (blue dotted line), $t > 2.5$ Gyr (green dashed line).

An obvious feature in Fig. 7 is that clusters with $R > 12$ kpc locate the upper envelope of the MD versus age, which may be related to the discrepancy of the metallicity gradient in Fig. 2. Here we adopt the $R = 11.5$ kpc as a division between the inner disk and the outer disk since it corresponds to the discrepancy of the metallicity gradient between the linear fit and the running average in Fig. 2. As shown in the left panel of Fig. 9, migration distances of clusters in the inner disk and the outer disk show different trends with R_g . The distribution of migration distance is not related to R_g in the inner disk where half of the clusters are in-situ, and the majority of the remaining clusters migrate outward with only 12 clusters (with young age of $t \leq 0.5$ Gyr) showing inward migration. In the outer disk, the migration distance increases with R_g , and only four clusters are born locally. The right panel of Fig. 9 shows R_b as a function of R_g . It can be seen that the birth sites of the inner and outer disk clusters are different: the R_b of the inner disk clusters are mainly distributed at 3 – 12 kpc, and those of the outer disk are mainly distributed at 8 – 12 kpc. There are no clusters born outside of 12.1 kpc in this sample, and most of the clusters in the outer disk have migrated outward to present locations. For clusters with $R_g < 11.5$ kpc, R_b increases with R_g ; this trend breaks when $R_g \sim 11.5$ kpc, R_b no longer increases with R_g but flattens. This flattening trend in the outer disk mainly occurs in clusters with age > 1 Gyr. In addition, all outer disk clusters are born outside of 7.4 kpc, and only Berkeley 36 was born within the solar radius. Only two old clusters (Berkeley 17 and Berkeley 36) are born within the solar radius and have a migration distance greater than 4 kpc. Their R_g are 10.9 and 11.8 kpc respectively and they are all old open clusters (7.2 and 6.8 Gyr). The above results indicate the breaking metallicity gradient is caused by the existence of old open clusters (> 1 Gyr) in the outer disk beyond 11.5 kpc, which are born from the inner side and migrates to the current location. But clusters born within the solar radius may need a longer time to have a chance to migrate to the outer disk.

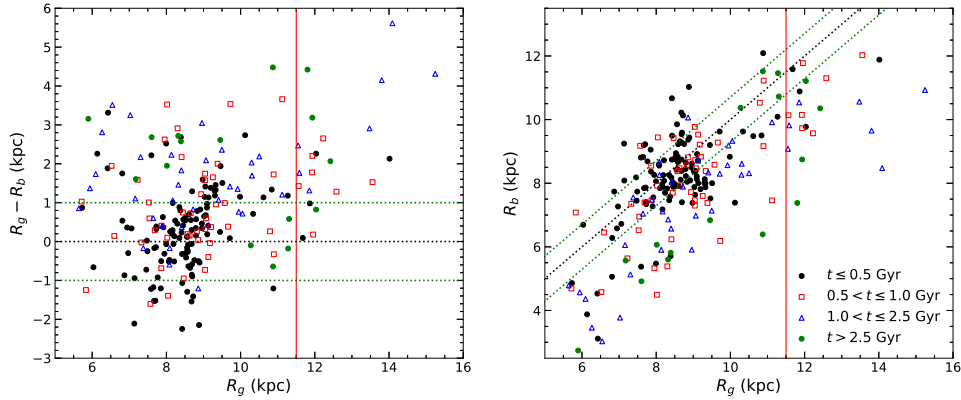


Figure 9. Left: The migration distance $R_g - R_b$ versus R_g for different age bins. The black dotted line indicates $R_g - R_b = 0$, the green dotted line indicates $R_g - R_b = 1$ or -1 kpc, and the red solid line indicates the boundary between the inner and outer disks, $R_g = 11.5$ kpc. Right: The R_b versus R_g for different age bins.

As can be seen in Fig. 9, more than half of the clusters in the inner disk of $R_g < 7$ kpc migrated outward to their current positions, which is higher than those near the solar radius. The R_b and R_g of these outward migrating clusters are 3 – 5 kpc and 6 – 7 kpc respectively. Since the clusters with $R_g < 7$ kpc are closer to the central bar, they will be more strongly affected by the coupling of the spiral arm and bar, and thus the effect of radial migration will be more obvious. According to Bovy et al. (2019) and Queiroz et al. (2020), the highest metallicity is not located in the Galactic center, but roughly at $R = 3 - 5$ kpc. According to Minchev et al. (2013), the co-rotation radius is 4.7 kpc, where radial migration is the most intense and produces inward migration as well as outward migration. Therefore, many metal-rich clusters migrated to $R_g > 5$ kpc, which also led to the steepening of the metallicity gradient of the clusters with $R_g < 7$ kpc in Fig. 2.

3.5. MDF for migrators and in-situ clusters

It is interesting to investigate the metallicity distribution function (MDF) between migrators and in-situ clusters for different Galactic distances. Fig. 10 shows the MDF of the total sample (upper left), $R \leq 9$ (upper right), $9 < R \leq 12$ (lower left), $R > 12$ kpc (lower right) samples. As can be seen from the upper left panel, the metallicity range of the total sample is $-0.45 < [\text{Fe}/\text{H}] < 0.3$ dex, which is similar to the range of migrators and in-situ clusters. But clusters with super solar metallicity are mainly migrators, which form at the inner disk and migrate outward to their current locations. Due to the high star formation rate (SFR) and high metallicity of ISM in the inner disk, we would expect the difference between migrators and in-situ clusters is more significant at the metal-rich end, which is also shown in the upper left panel of Fig. 10.

The MDF of in-situ clusters is picked at -0.05 dex, and has a long tail toward lower metallicities, indicating an obvious skewness. The MDF peak of the total sample is also at -0.05 dex, but the skewness is not obvious. The MDF of migrators has multiply peaks and tends to extend significantly toward super solar metallicity. The skewness of the total sample, migrators, and in-situ clusters are 0.1, 0.3, and -1.2 , respectively. The skewness of the MDF of the total sample toward the low

metallicities disappears due to the contribution of the less skewness distributed migrators, and the peak are determined by in-situ clusters.

We further divide the sample into three groups according to Galactic radial distance R , $R \leq 9$ kpc, $9 < R \leq 12$ kpc, and $R > 12$ kpc. For the largest group of $R \leq 9$ kpc, the MDF peak of the total sample is still determined by in-situ clusters, and migrators were evenly distributed at $-0.1 - 0.2$ dex. The inward migrators mainly distribute in $-0.25 - -0.05$ dex, while the outward migrators mainly distribute in $-0.05 - 0.3$ dex, and there are few in-situ clusters where $[\text{Fe}/\text{H}] > 0.05$ dex. For clusters with $9 < R \leq 12$ kpc, the characteristics of MDF are basically the same as those with $R \leq 9$ kpc: peak value of the overall sample is determined by in-situ clusters, and the high-metallicity tail is determined by migrators. The difference is that the number of inward migrating clusters is very small, which has little effect on MDF. For clusters with $R > 12$ kpc, almost all clusters are outward migrators.

Loebman et al. (2016) used a high-resolution N-body + SPH simulation and APOGEE DR12 data to study the effect of radial migration on the MDF of field stars. They proposed that the radial migration caused the MDF to be negatively skewed at small R_{gc} and positively skewed at large R_{gc} . Due to the small number of open clusters in our sample, we cannot analyze the skewness of MDF in each R bin to compare it with the MDF of field stars. But the same result is that their peaks are all determined by in-situ clusters, and the high-metallicity tail is almost all contributed by migrators (see their Figure 4).

3.6. Migration distance for the three sequences

It is found the metallicity of intermediate-age open clusters is higher than that of young open clusters at a given Galactocentric distance (e.g. Jacobson et al. 2016; Netopil et al. 2016; Spina et al. 2017), which correspond to the upper sequence in Fig. 5. This sequence is composed of clusters that migrate outward as shown in Fig. 11, and has an extensive R_g range from the inner disk (5.5 kpc) to the outer disk (up to 14.5 kpc), i.e. the whole Galactic disk. The lower sequence is mainly composed of inwardly migrated clusters, and the R_g distribution has a cutoff at 12.5 kpc, which causes the radial metallicity gradient to break out. That is, there is a lack of inwardly migrated clusters in the outer disk (see Fig. 9), while the outwardly migrated clusters from more metal-rich inner disk can reach farther, increasing the mean metallicity of the outer disk and thus the radial metallicity gradient flattening out. In addition, radial migration leads to dispersion in radial metallicity distribution of open clusters, as suggested by Anders et al. (2017). As more clusters are migrating outward than those migrating inward, the number of clusters in the inner disk reduces. They also proposed that non- and inward-migrating clusters are disrupted faster, which can explain the present-day radial metallicity distribution. According to the inside-out formation mechanism, the number density of stars in the inner disk is higher, and open clusters are more easily to be disrupted due to collisions. As can be seen in Fig. 2, there are few open clusters with $R_g < 6$ kpc in our samples.

The above analysis shows different effect of radial migration between the inner disk and outer disk with a division around ~ 11.5 kpc. According to Minchev et al. (2013), the coupled interaction between the Galactic bar and spiral arms could invoke very effective radial migration. This mechanism play an important role in the inner disk, since the Galactic bar locates in the inner Galaxy of $R < 5$ kpc (e.g. Bovy et al. 2019). For the outer disk far away from the bar, the bar-spiral-arm mechanism may still work, but the impact is less as compared with the inner disk. Meanwhile, there may be other mechanisms at work in the outer disk, such as minor merger (Quillen et al. 2009), which will

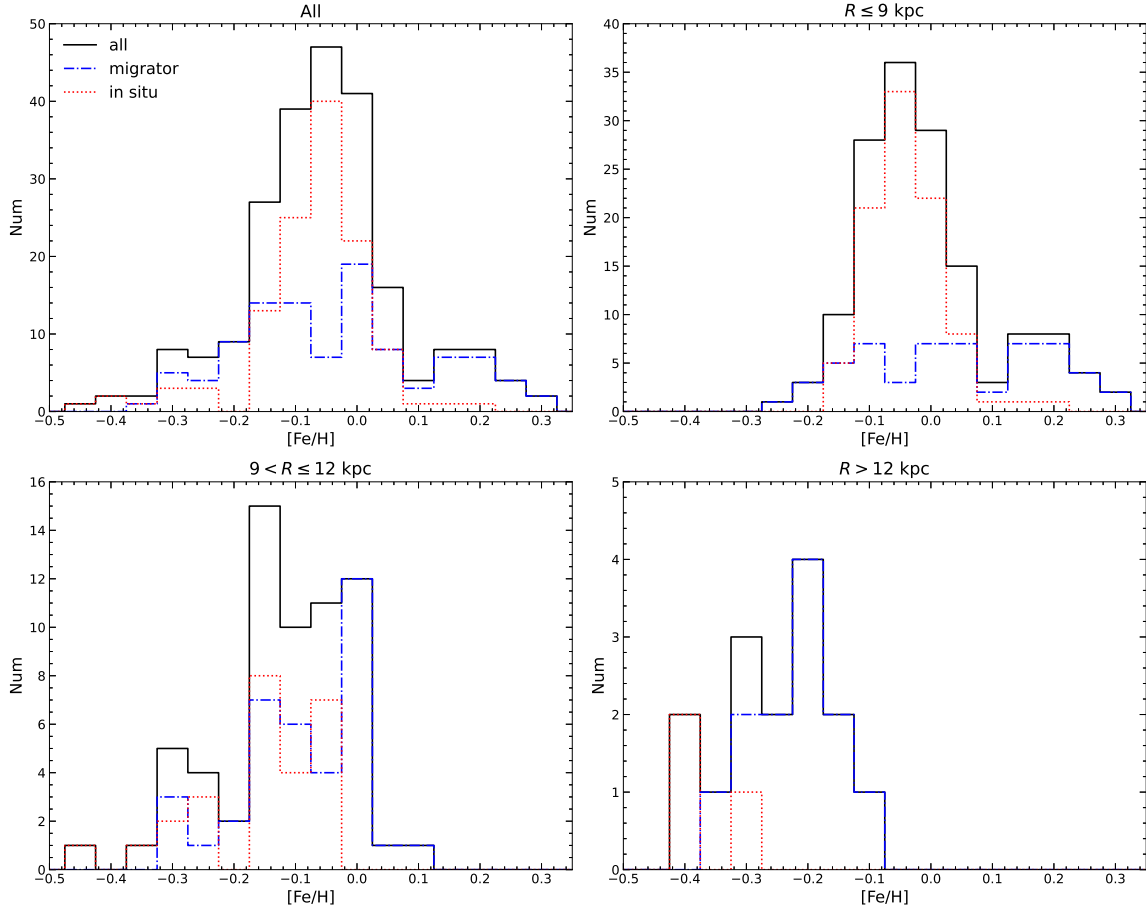


Figure 10. Metallicity distribution of the total sample (upper left), $R \leq 9$ (upper right), $9 < R \leq 12$ (lower left), $R > 12$ kpc (lower right) samples. In each panel, all clusters, migrators, and in-situ clusters are represented by black solid line, blue chain line, and red dotted line.

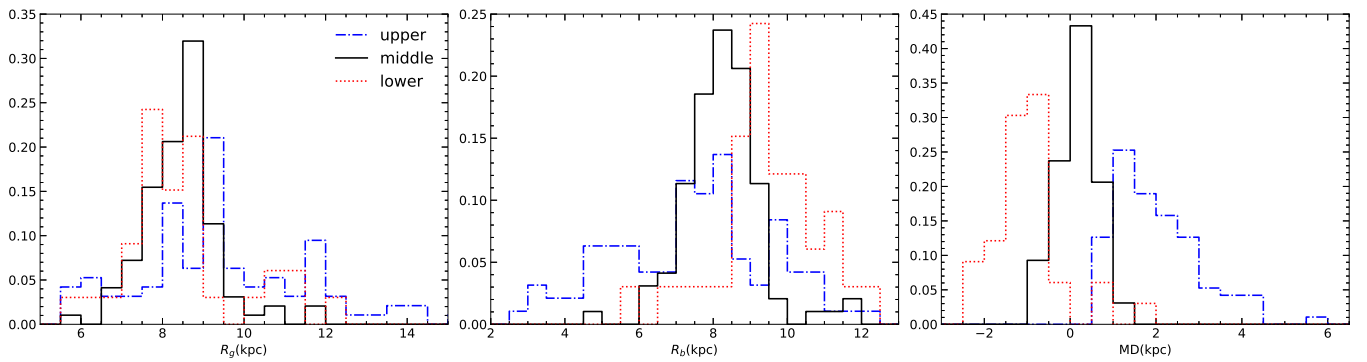


Figure 11. The distribution of R_g (left), R_b (middle), and MD (right) of the three sequences. In each panel, upper, middle, and lower sequences are represented by blue chain line, black solid line, and red dotted line.

cause many special clusters to appear in the outer disk. But our sample is limited to $|Z| < 0.5$ kpc, so these special clusters are basically excluded.

4. SPECIAL OPEN CLUSTERS THROUGHOUT THE GALACTIC DISK

As discussed in Sect. 3.1, Berkeley 32 is a special cluster with underabundant metallicity for its location. Specifically, Berkeley 32 has a metallicity of -0.34 dex, and its age is 4.9 Gyr. It is located at $R = 11.0$ kpc, close to the boundary between the inner and outer disks. Its birth radius is 9.6 kpc and its guiding center radius is $R_g = 8.8$ kpc, and thus it is an in-situ cluster. However, its radial oscillation is very large, which is 4.9 kpc. Based on these data, it is blurring, rather than churning, that affects Berkeley 32.

We also found three special clusters in the left panel of Fig. 7: King 2, Trumpler 5, and IC 166. The same as Berkeley 32, Trumpler 5 and King 2 are a few in-situ clusters older than 4 Gyr with $R_g - R_b$ of 0.8 and -0.1 kpc, respectively. Therefore, there are still a few clusters that have not to leave their birth location after 4 Gyr. King 2 has a similar situation to Berkeley 32: it has $[\text{Fe}/\text{H}] = -0.36$, age = 4.1 Gyr, $R = 11.4$ kpc, $R_g = 10.3$ kpc, $R_b = 10.4$ kpc. It also has a large radial oscillation of 3.8 kpc, so the effect of blurring is larger than that of churning for King 2. Trumpler 5 has a different situation: either churning or blurring has little effect on it. It has typical thin disk kinematics, $e = 0.08$, $Z_{max} = 0.1$ kpc, which leads to radial oscillation of only 1.9 kpc. Donati et al. (2015) analyzed the abundances of several elements of Trumpler 5 using high-resolution UVES spectra, and compared them with the abundance ratios of field stars with the same metallicity, and concluded that Trumpler 5 has a typical thin-disk abundance ratio (see their Figure 10). Trumpler 5 has an age of 4.3 Gyr and locates at $R = 11.3$ kpc. Buck (2020) proposed that the merger brought fresh metal-poor gas to dilute ISM's metallicity in the galactic outskirts starting from about 7 Gyr ago, resulting in the formation of a large number of low- α metal-poor stars. According to the simulation of Buck (2020), the age, location, $[\text{Fe}/\text{H}]$, and $[\alpha/\text{Fe}]$ of Trumpler 5 indicates that it may be born after the merger of metal-poor gas.

IC 166 is currently in the outer disk, $R = 12.3$ kpc, $R_g = 14.1$ kpc, but its metallicity is relatively high, is -0.1 dex. Hence it becomes the most metal-rich cluster in the outer disk in the sample. With 1.3 Gyr age, $R_b = 8.5$ kpc, it has a high migration rate of 4.3 kpc/Gyr. Also, it shows a large radial oscillation (4.6 kpc) due to blurring. In short, this is a metal-rich cluster in the outer disk with strong effect from both churning and blurring due to unknown mechanism. Using APOGEE data, Schiappacasse-Ulloa et al. (2018) calculated the eight chemical abundance species (Mg, Ca, Ti, Si, Al, K, Fe, and Mn) for IC 166, and suggested that the cluster lies in the low- α sequence of the canonical thin disk.

In summary, for some old (age > 1 Gyr) open clusters located at $R > 11$ kpc, blurring also plays an important role, such as Berkeley 32, King 2, and IC 166. In addition, there are clusters that either churning or blurring has little effect on it, such as Trumpler 5, which may be born after the merger of metal-poor gas in the galactic outskirts. These special clusters reveal the complicated history of the evolution of the outer Galactic disk.

5. CONCLUSIONS

Metallicity, age, and kinematics for a sample of 225 open clusters are compiled from the literature to study the radial migration of the thin disk of the Galaxy. The metallicity and radial velocity data come from the catalog of open clusters of Netopil et al. (2016) (only metallicity, based on a variety of high-resolution spectroscopic data), Soubiran et al. (2018), (only radial velocity, based on Gaia DR2), Casali et al. (2019) (based on Gaia-ESO), Donor et al. (2020) (based on APOGEE

DR16), [Spina et al. \(2021\)](#) (based on GALAH+ and APOGEE DR16) and SPA survey, supplemented by the LAMOST DR7 data. The age data and the rest of the kinematics parameters are from [Cantat-Gaudin et al. \(2020\)](#) based on Gaia DR2.

Based on the high-resolution spectroscopic data of clusters with age < 0.5 Gyr, we calculate the present-day metallicity gradient by linear fit to open clusters in the solar neighborhood, and it is -0.074 ± 0.007 dex/kpc. The systematic difference between the radial metallicity profile of ISM in [Minchev et al. \(2018\)](#) and our sample is modified by the present-day metallicity gradient, and the birth radius is calculated as well as the migration distance $R_g - R_b$. According to the criterion of $|R_g - R_b| > 1$ kpc, 46% of open clusters have migrated. We divide clusters into three sequences in the $[\text{Fe}/\text{H}]$ versus R_g diagram according to their distribution along the present-day metallicity gradient: upper (above the fitting line), middle (near the fitting line), and lower (under the fitting line). These three sequences of clusters are mainly outward migrators, in-situ clusters, and inward migrators, respectively. This indicates that the metallicity scatters in the radial metallicity distribution of open clusters is mainly caused by radial migration, not only by the uncertainty in metallicity. The $R_g - R_b$ and $|R - R_g|$ of clusters both increase with age, but the most effective time of radial migration occurs when the age is less than 3 Gyr. At age > 3 Gyr, the migration rate becomes lower. Therefore, the radial migration of open clusters is closely related to age, and old clusters generally migrate outward.

The radial migration takes effect in an extensive range of the Galactic disk. There are many more clusters migrating outward than inward, and their distribution range is 5.5–14.5 kpc, which is almost the same as the distribution range of the overall sample, while the inwardly migrating clusters are distributed in 5.5–12.5 kpc. This explains why the radial metallicity distribution of open clusters has obvious scatter throughout the disk. Besides, the flattening of the metallicity gradient of the open clusters outside 11.5 kpc can be explained by the absence of the lower sequence clusters.

The determination of the boundary between the inner and outer disks of the Milky Way is complicated, and different works give different results (e.g. 10 kpc in [Haywood et al. 2013, 2016](#)). In our work, the break of the radial metallicity gradient of open clusters is found to be 11.5 kpc where the linear function starts to deviate from the running average curve, and the gradient flatten out. Furthermore, the distribution of inwardly migrating clusters has a cutoff at around 12.5 kpc. We thus suggested that 11.5 kpc is the boundary between the inner and outer disks based on the churning of open clusters. We propose that the main mechanism of radial migration by the coupling of the bar and spiral arms ([Minchev et al. 2013](#)) works in both the inner and outer disks, but within 11.5 kpc, this mechanism is more effective. There are both inwardly and outwardly migrating clusters in the inner disk, but the clusters in the outer disk almost all migrate from the inner disk, and they are almost no young clusters. Some complex extra mechanisms join the main mechanism in the outer disk and near the boundary, which will cause some special clusters to appear, such as Berkeley 32, King 2, IC 166, and Trumpler 5.

This study is supported by the National Natural Science Foundation of China under grants No. 11988101, 11625313, 11890694, 11973048, 11927804, National Key R&D Program of China No. 2019YFA0405502, and the 2-m Chinese Space Survey Telescope project. This work is also supported by the Astronomical Big Data Joint Research center, co-founded by the National Astronomical Observatories, Chinese Academy of Sciences and the Alibaba Cloud.

Guoshoujing Telescope (the Large Sky Area Multi-Object Fiber Spectroscopic Telescope LAMOST) is a National Major Scientific Project built by the Chinese Academy of Sciences. Funding for the project has been provided by the National Development and Reform Commission. LAMOST is operated and managed by the National Astronomical Observatories, Chinese Academy of Sciences.

This work has made use of data from the European Space Agency (ESA) mission Gaia (<https://www.cosmos.esa.int/gaia>), processed by the Gaia Data Processing and Analysis Consortium (DPAC, <https://www.cosmos.esa.int/web/gaia/dpac/consortium>). Funding for the DPAC has been provided by national institutions, in particular the institutions participating in the Gaia Multilateral Agreement.

REFERENCES

- Abuter, R., Amorim, A., Anugu, N., et al. 2018, *A&A*, 615, L15
- Anders, F., Chiappini, C., Minchev, I., et al. 2017, *A&A*, 600, A70
- Balsler, D. S., Wenger, T. V., Anderson, L., & Bania, T. 2015, *ApJ*, 806, 199
- Bennett, M., & Bovy, J. 2019, *MNRAS*, 482, 1417
- Bergemann, M., Ruchti, G., Serenelli, A., et al. 2014, *A&A*, 565, A89
- Bird, J. C., Kazantzidis, S., & Weinberg, D. H. 2012, *MNRAS*, 420, 913
- Bovy, J. 2015, *ApJS*, 216, 29
- Bovy, J., Leung, H. W., Hunt, J. A., et al. 2019, *MNRAS*, 490, 4740
- Buck, T. 2020, *MNRAS*, 491, 5435
- Cantat-Gaudin, T., Anders, F., Castro-Ginard, A., et al. 2020, *A&A*, 640, A1
- Carraro, G., & Chiosi, C. 1994, *A&A*, 287, 761
- Casali, G., Magrini, L., Tognelli, E., et al. 2019, *A&A*, 629, A62
- Casali, G., Magrini, L., Frasca, A., et al. 2020, *A&A*, 643, A12
- Chen, Y., & Zhao, G. 2020, *MNRAS*, 495, 2673
- Chiappini, C. 2008, *Proceedings of the International Astronomical Union*, 4, 191
- Comparetta, J., & Quillen, A. C. 2012, *arXiv preprint arXiv:1207.5753*
- Cui, X.-Q., Zhao, Y.-H., Chu, Y.-Q., et al. 2012, *RAA*, 12, 1197
- De Silva, G. M., Freeman, K. C., Bland-Hawthorn, J., et al. 2015, *MNRAS*, 449, 2604
- Deng, L.-C., Newberg, H. J., Liu, C., et al. 2012, *RAA*, 12, 735
- Dias, W., Alessi, B., Moitinho, A., & Lépine, J. 2002, *A&A*, 389, 871
- Donati, P., Coccozza, G., Bragaglia, A., et al. 2015, *MNRAS*, 446, 1411
- Donor, J., Frinchaboy, P. M., Cunha, K., et al. 2020, *AJ*, 159, 199
- D’Orazi, V., Oliva, E., Bragaglia, A., et al. 2020, *A&A*, 633, A38
- Eilers, A.-C., Hogg, D. W., Rix, H.-W., & Ness, M. K. 2019, *ApJ*, 871, 120
- Frasca, A., Alonso-Santiago, J., Catanzaro, G., et al. 2019, *A&A*, 632, A16
- Friel, E. D., Jacobson, H. R., & Pilachowski, C. A. 2010, *AJ*, 139, 1942
- Gaia Collaboration. 2018, *A&A*, 616
- Genovali, K., Lemasle, B., Bono, G., et al. 2014, *A&A*, 566, A37
- Gilmore, G., Randich, S., Asplund, M., et al. 2012, *Messenger*, 147, 25
- Gómez, F. A., Minchev, I., Villalobos, Á., O’Shea, B. W., & Williams, M. E. 2012, *MNRAS*, 419, 2163
- Haywood, M., Di Matteo, P., Lehnert, M. D., Katz, D., & Gómez, A. 2013, *A&A*, 560, A109
- Haywood, M., Lehnert, M., Di Matteo, P., et al. 2016, *A&A*, 589, A66
- Helmi, A., Babusiaux, C., Koppelman, H. H., et al. 2018, *Nature*, 563, 85
- Jacobson, H. R., Friel, E., Jílková, L., et al. 2016, *A&A*, 591, A37
- Loebman, S. R., Debattista, V. P., Nidever, D. L., et al. 2016, *ApJL*, 818, L6
- Majewski, S. R., Schiavon, R. P., Frinchaboy, P. M., et al. 2017, *AJ*, 154, 94
- Minchev, I., Chiappini, C., & Martig, M. 2013, *A&A*, 558, A9
- . 2014, *A&A*, 572, A92
- Minchev, I., & Famaey, B. 2010, *ApJ*, 722, 112

- Minchev, I., Famaey, B., Combes, F., et al. 2011, *A&A*, 527, A147
- Minchev, I., Anders, F., Recio-Blanco, A., et al. 2018, *MNRAS*, 481, 1645
- Netopil, M., Paunzen, E., Heiter, U., & Soubiran, C. 2016, *A&A*, 585, A150
- Nieva, M.-F., & Przybilla, N. 2012, *A&A*, 539, A143
- Nissen, P. E., & Gustafsson, B. 2018, *A&ARv*, 26, 1
- Queiroz, A., Chiappini, C., Perez-Villegas, A., et al. 2020, arXiv preprint arXiv:2007.12915
- Quillen, A. C., Minchev, I., Bland-Hawthorn, J., & Haywood, M. 2009, *MNRAS*, 397, 1599
- Quillen, A. C., Nolting, E., Minchev, I., De Silva, G., & Chiappini, C. 2018, *MNRAS*, 475, 4450
- Reid, M., Menten, K., Brunthaler, A., et al. 2014, *ApJ*, 783, 130
- Sánchez, S., Galbany, L., Pérez, E., et al. 2015, *A&A*, 573, A105
- Schiappacasse-Ulloa, J., Tang, B., Fernández-Trincado, J., et al. 2018, *AJ*, 156, 94
- Schönrich, R., Binney, J., & Dehnen, W. 2010, *MNRAS*, 403, 1829
- Sellwood, J. A., & Binney, J. 2002, *MNRAS*, 336, 785
- Soubiran, C., Cantat-Gaudin, T., Romero-Gómez, M., et al. 2018, *A&A*, 619, A155
- Spina, L., Randich, S., Magrini, L., et al. 2017, *A&A*, 601, A70
- Spina, L., Ting, Y.-S., De Silva, G. M., et al. 2021, *MNRAS*, 503, 3279
- Yong, D., Carney, B. W., & Friel, E. D. 2012, *AJ*, 144, 95
- Zhong, J., Chen, L., Wu, D., et al. 2020, *A&A*, 640, A127
- Zinchenko, I., Pilyugin, L., Grebel, E., Sánchez, S., & Vílchez, J. 2016, *MNRAS*, 462, 2715